

Simulating the All-Order Strong Coupling Expansion IV: $CP(N - 1)$ as a loop model

Uli Wolff*

Institut für Physik, Humboldt Universität
Newtonstr. 15
12489 Berlin, Germany

Abstract

We exactly reformulate the lattice $CP(N - 1)$ spin model on a D dimensional torus as a loop model whose configurations correspond to the complete set of strong coupling graphs of the original system. A Monte Carlo algorithm is described and tested that samples the loop model with its configurations stored and manipulated as a linked list. Complete absence of critical slowing down and correspondingly small errors are found at $D = 2$ for several observables including the mass gap. Using two different standard lattice actions universality is demonstrated in a finite size scaling study. The topological charge is identified in the loop model but not yet investigated numerically.

HU-EP-10/01

SFB/CCP-10-04

*e-mail: uwolff@physik.hu-berlin.de

1 Introduction

For a few simple lattice field theories Monte Carlo simulation algorithms are known that are virtually free of critical slowing down. In these cases we have an almost qualitatively improved control over approaching the universal continuum or scaling limit which is essential for particle as well as statistical physics applications. One important line of such developments started from the Swendsen Wang cluster algorithm [1] for Potts, and in particular Ising models, in arbitrary dimension. In [2] the present author has shown how via embedded Ising spins these techniques can be extended to $O(N)$ invariant sigma models. This has led to numerous high precision simulations close to criticality in the literature. Unfortunately efforts to widen the applicability to other theories have since ended in frustration in many cases. A well known example concerning the $CP(N-1)$ model family is discussed in [3]. Some theoretical understanding of the restriction to $O(N)$ is given in [4]. Significant progress in the simulation of $CP(N-1)$ models has nevertheless been made in the sequel, for example with the non-recursive multigrid ('unigrid') method in [5], [6]. In [7], [8] an interesting but somewhat indirect method via quantum models and their reduction from higher dimension was presented. Nonetheless $CP(N-1)$ systems seem to remain a challenging testing ground for hopefully more systematically generalizable attempts to boost the efficiency of the numerical evaluation of lattice field theory.

A completely different recent research programme is based on the proposal of a Monte Carlo summation of the strong coupling series (in a certain simple form) which replaces the sampling of lattice field configurations. For many models of interest this series converges for any given *finite* volume and choice of parameters, and the in general infinite set of strong coupling graphs may be considered as an equivalent non-perturbative representation of the original lattice model. 'Worm' algorithms generalizing those described in [9] were the essential tool to allow for an efficient simulation of this ensemble. In this formulation criticality means that large graphs are important, which are far too numerous for systematic evaluation. The question if a Monte Carlo procedure can efficiently sample a sufficient subset seems rather different from the problem of collectively updating long distance correlated fields. Little other means than numerical experiments are presently available to answer this distinct and open question. We here extend the recent series of papers [10], [11], [12] to give an affirmative answer also for $CP(N-1)$.

In particular in [10] many details for the treatment of non-Abelian models have been developed that are similar here. Therefore we have to constantly refer to this work and the present paper could not really become self-contained without excessive repetition. On the other hand here further progress is made for the simulation method that can be used to also render the $O(N)$ model simulations even more efficient than what was described in [10].

The present paper is organized as follows. In section 2. we formulate the $\text{CP}(N - 1)$ model in several discretizations and derive the equivalent loop models. For their simulation an algorithm is described in section 3 and numerically applied in section 4. In section 5. the loop formulation is generalized to include the θ parameter coupled to the topological charge, but related numerical experiments are left to possible future publications. We end in section 6. with some brief conclusions.

2 $\text{CP}(N - 1)$ model as a loop model

2.1 Explicit gauge field formulation

The $\text{CP}(N - 1)$ model is formulated with spins on lattice sites with values in a complex $N - 1$ dimensional projective space. They may be represented by one-dimensional projectors or by complex N -component unit vectors $\phi(x) \in \mathbb{C}^N$, $|\phi| = 1$, whose phases are irrelevant. One of the standard lattice actions [13] in use can be written as

$$-S[\phi, U] = \beta \sum_{x\mu} [U(x, \mu) \phi^\dagger(x) \phi(x + \hat{\mu}) + U^{-1}(x, \mu) \phi^\dagger(x + \hat{\mu}) \phi(x)]. \quad (1)$$

We here sum over all links of a hypercubic periodic lattice in D dimensions with extent L_μ in direction $\mu = 0, 1, \dots, D - 1$. We use lattice units in which the L_μ are integer and $V = \prod L_\mu$ is the number of lattice cells or sites. In addition to the spin field ϕ a $U(1)$ gauge field $U(x, \mu)$ is included which can absorb local phase transformations of $\phi(x)$. There also is a global $SU(N)$ invariance with ϕ in the fundamental representation. In a first step we consider U as a given ‘background’ field over which we integrate later. We define the following partition function with two contracted adjoint composite insertions

$$Y[u, v; U] = \int \left[\prod_z d\mu(\phi(z)) \right] e^{-S[\phi, U]} \phi^\dagger(u) \lambda^a \phi(u) \phi^\dagger(v) \lambda^a \phi(v) \quad (2)$$

where $d\mu$ is the normalized invariant measure on the $2N - 1$ dimensional sphere of $2N$ real component unit vectors made from the real and imaginary part of ϕ . The generalized Pauli-Gell-Mann matrices λ^a with $a = 1, 2, \dots, N^2 - 1$ are a basis for traceless $N \times N$ matrices that obey the normalization condition

$$\text{tr}(\lambda^a \lambda^b) = 2\delta^{ab}. \quad (3)$$

Using the easily proven completeness relation

$$\lambda_{\alpha\beta}^a \lambda_{\gamma\delta}^a = 2 \left(\delta_{\alpha\delta} \delta_{\beta\gamma} - \frac{1}{N} \delta_{\alpha\beta} \delta_{\gamma\delta} \right) \quad (4)$$

we may verify that our normalization is such that for coinciding $u = v$

$$Y[u, u; U] = 2(1 - 1/N) \int \left[\prod_z d\mu(\phi(z)) \right] e^{-S[\phi, U]} \quad (5)$$

holds and thus the ordinary partition function emerges up to a known factor.

The single site generating function immediately follows from the one of the $O(N)$ model [10]

$$\int d\mu(\phi) e^{j^\dagger \phi + \phi^\dagger j} = \sum_{n=0}^{\infty} F[n; N] (j^\dagger j)^n \quad (6)$$

with

$$F[n; N] = \frac{\Gamma(N)}{n! \Gamma(N + n)}. \quad (7)$$

On each link $x\mu$ ($y = x + \hat{\mu}$) we double-expand

$$e^{\beta[U\phi^\dagger(x)\phi(y) + U^{-1}\phi^\dagger(y)\phi(x)]} = \sum_{k, \bar{k}=0}^{\infty} \frac{\beta^{k+\bar{k}}}{k! \bar{k}!} U^{k-\bar{k}} (\phi^\dagger(x)\phi(y))^k (\phi^\dagger(y)\phi(x))^{\bar{k}}, \quad (8)$$

then promote the integers to link fields $k(x, \mu), \bar{k}(x, \mu)$ and also introduce the differences

$$j_\mu(x) \equiv j(x, \mu) = k(x, \mu) - \bar{k}(x, \mu). \quad (9)$$

Auxiliary fields

$$d(z) = \sum_{\mu} \bar{k}(z - \hat{\mu}, \mu) + k(z, \mu) + \delta_{z,u} + \delta_{z,v} \quad (10)$$

and

$$\bar{d}(z) = \sum_{\mu} k(z - \hat{\mu}, \mu) + \bar{k}(z, \mu) + \delta_{z,u} + \delta_{z,v} \quad (11)$$

count the number of factors ϕ^\dagger and ϕ at each site in an expansion term. The measure (6) is $U(1)$ invariant such that nonzero contributions only result if $d(z) = \bar{d}(z)$ holds at all sites. This condition is equivalent to the vanishing divergence or flux conservation

$$d(x) - \bar{d}(x) = \partial_\mu^* j_\mu(x) = 0 \quad (12)$$

where ∂_μ^* is the nearest neighbor backward derivative.

The relevant integral over ϕ now is

$$Y[u, v; U] = \sum_{k, \bar{k}} \prod_{x\mu} \left[\frac{\beta^{k(x, \mu) + \bar{k}(x, \mu)}}{k(x, \mu)! \bar{k}(x, \mu)!} U^{j(x, \mu)} \right] \int \left[\prod_z d\mu(\phi(z)) \right] \cdots \quad (13)$$

$$\dots \phi^\dagger(u) \lambda^a \phi(u) \phi^\dagger(v) \lambda^a \phi(v) \prod_{y\nu} (\phi^\dagger(y) \phi(y + \hat{\nu}))^{k(y,\nu)} (\phi^\dagger(y + \hat{\nu}) \phi(y))^{\bar{k}(y,\nu)}.$$

Precisely as in [10] this spin integral can now be performed by replacing all ϕ, ϕ^\dagger by derivatives with respect to sources $\partial/\partial j^\dagger, \partial/\partial j$ and then using (6) on all sites. All $SU(N)$ indices get contracted and the various terms correspond to strong coupling graphs on the lattice. On each link we draw $k(x, \mu)$ lines with arrows in the positive direction and $\bar{k}(x, \mu)$ lines with opposite arrows. At each site z we again imagine all possible ways to saturate all derivatives as a ‘switchboard’ that connects (contracts) all surrounding lines pairwise with each other, always an incoming to an outgoing one. This involves the weight $F(d(z); N)$ from the measure at that site. The ‘connectors’ are regarded as 2-vertices joining pairs of lines at sites. In this way oriented closed loops arise around which the contractions in internal space contribute a factor N per loop to the total weight. Two (chains of) lines connect pairwise the four inserted spins at u and v , they end in four 1-vertices. These lines are open geometrically (unless $u = v$) and are saturated in internal space by the λ matrices. Because these are traceless there is only one nonzero pairing of the four spins: a positively oriented line pointing from a u -spin $[\phi^\dagger(u)]$ to a v -spin $[\phi(v)]$ and the other one from v to u . The result of these contractions is a factor $2(N^2 - 1)$. In analogy to the $O(N)$ model in [10] we call these lines active loops, distinguished as the uv -loop and the vu -loop, as opposed to the remaining passive loops. Either active loop is called trivial if for $u = v$ it entirely lives on that site, i.e. it has no lines and 2-vertices. We now regard $Y[u, v; U]$ as the sum over all possible loop graphs $\Lambda \in \bar{\mathcal{L}}_2$ of which each consists of many arbitrarily overlapping, intersecting and backtracking oriented closed loops plus the two active loops ending in 1-vertices at u and v . At this stage we consider k, \bar{k}, u, v as functions of Λ . All graphs in $\bar{\mathcal{L}}_2$ satisfy (12). After counting the multiplicity of the terms corresponding to each graph in the way discussed in [10] we arrive at the remarkably simple form

$$\mathcal{Y}[U] = C \sum_{u,v} \rho^{-1}(u - v) Y[u, v; U] = \sum_{\Lambda \in \bar{\mathcal{L}}_2} \rho^{-1}(u - v) W[\Lambda] N^{|\Lambda|} \prod_{x\mu} U^{j(x,\mu)} \quad (14)$$

with the weight

$$W[\Lambda] = \frac{1}{\mathcal{S}[\Lambda]} \left[\prod_{x\mu} \beta^{k(x,\mu) + \bar{k}(x,\mu)} \right] \prod_z \frac{\Gamma(N)}{\Gamma(N + d(z))}, \quad C^{-1} = 2(1 - 1/N^2). \quad (15)$$

In the exponent $|\Lambda|$ is the number of closed loops in the configuration Λ (including the two active ones in our convention). The factor $\mathcal{S}[\Lambda]$ is the symmetry factor of the graph introduced in the *erratum* to [10]. The strictly positive weight ρ with the normalization $\rho(0) = 1$ has been first discussed in [11] and will be chosen to our convenience later.

In the standard $\text{CP}(N-1)$ model one now integrates over all $U(x, \mu)$ independently link by link with the normalized $U(1)$ measure. This enforces the constraint $j(x, \mu) = 0$ in (14) on all links. We call this subset of graphs $\mathcal{L}_2 \subset \overline{\mathcal{L}}_2$. The flux represented by the arrows now has to vanish identically on all links instead of just being conserved at the sites. Then the loop partition function becomes

$$\mathcal{Z} = \int DU \mathcal{Y}[U] = \sum_{\Lambda \in \mathcal{L}_2} \rho^{-1}(u-v) W[\Lambda] N^{|\Lambda|}. \quad (16)$$

2.2 Quartic action formulation

A second popular action [13] for the $\text{CP}(N-1)$ model contains only the field ϕ with the action

$$-S_q[\phi] = 2\beta_q \sum_{x\mu} |\phi^\dagger(x)\phi(x + \hat{\mu})|^2. \quad (17)$$

If we start from S_q , the same steps as above immediately lead to the locally fluxless ($k \equiv \bar{k}$) graphs \mathcal{L}_2

$$\mathcal{Z}_q = \sum_{\Lambda \in \mathcal{L}_2} \rho^{-1}(u-v) W_q[\Lambda] N^{|\Lambda|} \quad (18)$$

with the weight, modified by the slightly different multiplicities,

$$W_q[\Lambda] = \frac{1}{\mathcal{S}[\Lambda]} \left[\prod_{x\mu} [2\beta_q]^{k(x,\mu)} k(x, \mu)! \right] \prod_z \frac{\Gamma(N)}{\Gamma(N + d(z))}. \quad (19)$$

For either action the relation between the two point correlation of the original spin model and the ensemble (16) or (18) is easy to establish. With double angle expectation values defined by [$W \rightarrow W_q$ for (18)]

$$\langle\langle \mathcal{O}(\Lambda) \rangle\rangle = \frac{1}{\mathcal{Z}} \sum_{\Lambda \in \mathcal{L}_2} \rho^{-1}(u-v) W[\Lambda] N^{|\Lambda|} \mathcal{O}(\Lambda) \quad (20)$$

we find

$$\langle\phi^\dagger(0)\lambda^a\phi(0)\phi^\dagger(x)\lambda^b\phi(x)\rangle = \rho(x) \frac{2\delta_{ab}}{N(N+1)} \frac{\langle\langle \delta_{u-v,x} \rangle\rangle}{\langle\langle \delta_{u,v} \rangle\rangle}. \quad (21)$$

In particular the susceptibility

$$\chi = \frac{1}{2} \sum_x \langle\phi^\dagger(0)\lambda^a\phi(0)\phi^\dagger(x)\lambda^a\phi(x)\rangle = \sum_x \left\{ \langle\text{tr}[\phi(0)\phi^\dagger(0)\phi(x)\phi^\dagger(x)]\rangle - \frac{1}{N} \right\} \quad (22)$$

can be measured as

$$\chi = \frac{N-1}{N} \frac{\langle\langle \rho(u-v) \rangle\rangle}{\langle\langle \delta_{u,v} \rangle\rangle}. \quad (23)$$

2.3 Adjoint formulation

The action S_q may also be rewritten completely in terms of adjoint composite fields

$$J^a(x) = \phi^\dagger(x)\lambda^a\phi(x). \quad (24)$$

We introduce

$$-S_a[\phi] = \beta_a \sum_{x\mu} J^c(x)J^c(x + \hat{\mu}) \quad (25)$$

but note that in the path integral we integrate over $\phi(x)$ as before. There is the trivial relation, again a consequence of (3),

$$S_a[\phi] = S_q[\phi]|_{\beta_q=\beta_a} + \frac{2DV}{N}\beta_a. \quad (26)$$

Thus S_q and S_a just differ by a constant shift, irrelevant for any correlation. In spite of this the all-order strong coupling expansions are far from identical. An expansion in powers of β_a using S_a would involve unoriented lines as for the $O(N)$ model. A major difference arises however from the measure that would be relevant in this case

$$\int d\mu(\phi)e^{b^a J^a} = \sum_{m,n=0}^{\infty} A[m,n;N](b^a b^a)^m (d_{abc} b^a b^b b^c)^n \quad (27)$$

with a source b^a . In the adjoint representation there is (for $N > 2$) a second invariant totally symmetric tensor beside δ_{ab} , namely

$$d_{abc} = \frac{1}{4} \text{tr}(\lambda^a \lambda^b \lambda^c + \lambda^b \lambda^a \lambda^c). \quad (28)$$

Thus this expansion is more complicated with both two point and three point vertices available to contribute. Only for $N = 2$ d_{abc} vanishes and the adjoint formulation falls back to the standard lattice formulation of the $O(3 = N^2 - 1)$ model as is well known. But even here S_q yields a new expansion and the numerical reproduction of $O(3)$ results in the $CP(1)$ formulation is non-trivial.

2.4 Nienhuis Boltzmann factor

In [10] we have locally modified the original Boltzmann factor by truncating its expansion on each bond by $k(x, \mu) \leq k_{\max}$. The original model is recovered for large k_{\max} but a particularly interesting case arises for $k_{\max} = 1$. Such modifications and the conjecture of universality still holding have been introduced into the

literature a long time ago [14], [15]. Truncating in the S_q formulation amounts to the replacement

$$e^{-S_q[\phi]} \rightarrow \mathcal{N}_q[\phi] = \prod_{x\mu} \left[1 + 2\tilde{\beta}_q |\phi^\dagger(x)\phi(x + \hat{\mu})|^2 \right]. \quad (29)$$

The adjoint translation reads

$$\mathcal{N}_q[\phi] = (1 + 2\tilde{\beta}_q/N)^{DV} \prod_{x\mu} \left[1 + \tilde{\beta}_a J^a(x) J^a(x + \hat{\mu}) \right] \quad (30)$$

with the adjoint Nienhuis coupling

$$\tilde{\beta}_a = \frac{\tilde{\beta}_q}{1 + 2\tilde{\beta}_q/N}. \quad (31)$$

For $\tilde{\beta}_q \geq 0$ we find $0 \leq \tilde{\beta}_a \leq N/2$. The criticality observed for $O(3)$ in [10] corresponds to large positive $\tilde{\beta}_a$ and $N = 2$. This is obviously not reached for positive $\tilde{\beta}_q$ but only as $\tilde{\beta}_q \nearrow (-N/2)$. We now turn to the possibilities of efficient Monte Carlo algorithms for the $CP(N - 1)$ loop model just outlined. We will however find this to be restricted to positive β_q and hence cannot at present implement the Nienhuis formulation as for the $O(3)$ model.

3 Simulation of the $CP(N - 1)$ loop model

3.1 Algorithm R for real N

We have arrived at a representation of the $CP(N - 1)$ model in terms of loops representing arbitrary strong coupling graphs. These configurations can be parameterized by linked lists as described in detail in [10] with only minor adjustments. One of the two possible orientations of each loop (for example column 2 of the list) is identified now with the physical orientation of lines of the present graphs. The flag in column 4 must now allow for three different values to distinguish between passive loops, the uv loop and the vu loop.

We first develop an algorithm to simulate the $CP(N - 1)$ loop ensemble (16). We define a number of separate update steps such that each of them fulfills detailed balance. They will then be iterated in some order as the final update procedure. The moves are all Metropolis proposals for which we quote a ratio q which yields the acceptance probability $\min(1, q)$. We encounter cases where our a priori proposal probabilities are not symmetric. To achieve detailed balance this needs to be compensated in q , which is then not just the ratio of the Boltzmann weights of the two configurations involved. This in particular applies to the inclusion of $\mathcal{S}[\Lambda]$ as discussed in the erratum to [10].

- I. Extension and retraction step: With probability $p_{\text{ext}} = 1/(1+r_{\text{ext}})$ we propose an extension step, otherwise the retraction step. In the extension branch we next choose with equal probability one of the $2D$ directions to move u to the corresponding neighbor \tilde{u} with a concurrent extension of both active loops. The proposal is accepted according to the ratio

$$q_{\text{ext}} = \frac{2D\beta^2 r_{\text{ext}}}{(N + d(\tilde{u}))(N + d(\tilde{u}) + 1)} \frac{\rho(u - v)}{\rho(\tilde{u} - v)}. \quad (32)$$

In the retraction branch u is pulled back over one link along the active loops with the ratio

$$q_{\text{ret}} = \frac{(N + d(u) - 1)(N + d(u) - 2)}{2D\beta^2 r_{\text{ext}}} \frac{\rho(u - v)}{\rho(\tilde{u} - v)} \quad (33)$$

if *both active loops* lead to the same neighbor \tilde{u} , otherwise no move is made.

- II. Re-route step: We here want to change the $SU(N)$ contraction or line connectivity structure at u . Such a move is only considered here if $u \neq v$ and $d(u) > 2$ holds.

- i. We pick one of the 2-vertices at u and propose to swap between the line pointing out of this 2-vertex and the uv loop emerging from its initial 1-vertex at u . For the q ratio we need to distinguish further sub-cases.
 - a) The chosen 2-vertex belongs to a passive loop. The latter then effectively gets inserted into the uv active loop at u , $|\Lambda|$ is reduced by one and we accept/reject with $q=1/N$.
 - b) The chosen 2-vertex belongs to the uv loop itself, which self-intersects at u . Then a section is detached from it forming a new passive loop, $|\Lambda|$ goes up by one, $q = N$.

No move is made if the chosen 2-vertex belongs to the vu loop.

- ii. As i. but the rôle of of the two active loops switched.

In figure 1 we try to graphically illustrate the elementary moves. We iterate these steps — and similar ones focussing on v instead of u — according to the scheme

$$1 \text{ Iteration} = (\text{I}_u \text{II}_u \text{I}_v \text{II}_v)^{N \times V/2}. \quad (34)$$

The ergodicity of this algorithm is shown as usual. One has to convince oneself that any graph can be built starting from the empty one by repeating the above moves. The empty graph is indeed the configuration from which we will start all simulations.

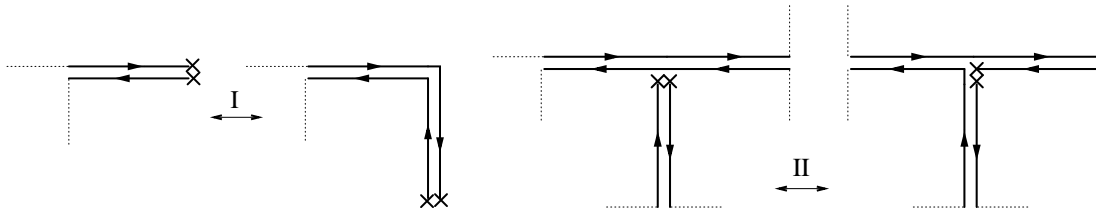


Figure 1: Illustration of elementary update steps I (left) and II (right). Dotted lines indicate the continuation with other parts of a graph Λ . The crosses are at the insertion site u .

For a simulation with the quartic action (17) we just have to replace (32) by

$$q'_{\text{ext}} = \frac{4D\beta_q r_{\text{ext}}(k(l) + 1)}{(N + d(\tilde{u}))(N + d(\tilde{u}) + 1)} \frac{\rho(u - v)}{\rho(\tilde{u} - v)} \quad (35)$$

and (33) by

$$q'_{\text{ret}} = \frac{(N + d(u) - 1)(N + d(u) - 2)}{4D\beta_q r_{\text{ext}} k(l)} \frac{\rho(u - v)}{\rho(\tilde{u} - v)}. \quad (36)$$

In the last two formulae l denotes the link between u and \tilde{u} , i.e. $l = (u, \mu)$ if $\tilde{u} = u + \hat{\mu}$ and $l = (\tilde{u}, \mu)$ if $\tilde{u} = u - \hat{\mu}$ with $\hat{\mu}$ denoting a unit vector in the positive μ direction.

In comparison with [10] a few changes can be noticed. The probability p_{ext} is new here. In [10] we have effectively chosen the special value $p_{\text{ext}} = 1/(2D+1)$. We found the greater flexibility here useful to prevent acceptance rates from getting small. In all runs reported about below we have taken $p_{\text{ext}} = 0.3$ and found unproblematic high acceptance rates. In addition there are no analogs of the steps Iii, Iiii and Iiii of [10]. We found that they are not essential and also the $O(N)$ algorithm may be simplified correspondingly. As a more technical change we have slightly modified the handling of the threefold linked list. As before two linkages allow to travel along loops in both directions while a third set of pointers allows to efficiently enumerate the vertices at a given lattice site. As we delete vertices (free list entries) in the retract step, we now immediately re-adjust all pointers including the site related ones.

3.2 Algorithm I for integer N

3.2.1 Why an improved method?

We have extensively run the algorithm just described and successfully reproduced numbers from the literature [16] [5] [6] for small and intermediate lattices ($L < 200$

in $D = 2, N = 4$) with permille errors using only moderate PC time. As for the $O(N)$ simulations in [10] we have found that integrated autocorrelation times *in units of iterations* typically stay below one in our timeseries of 10^6 iterations.

There nevertheless is a problem that is exacerbated here compared to $O(N)$. The moves described above seem to be superficially local with a fixed number of operations around u and v . For the reconnect II we have to know however if the 2-vertex that has been randomly chosen is part of a passive or an active loop, which represents nonlocal information that is locally available to us in the flag entry of the list [10]. The price to pay for this is that whenever sections of loops are detached or eaten up, these have to re-flagged. It turns out that thus, close to the continuum limit on large lattices, most of the CPU time is spent travelling around loops resetting flags. This problem was already discussed in [10]. It is more severe for $CP(N - 1)$ than for $O(N)$ because the loops are more numerous and probably longer for comparable correlation lengths and lattice sizes.

To diagnose the problem in more detail we have measured the loop-size distribution

$$\ell_n = \left\langle \left\langle \sum_{i=1}^{|\Lambda|} \delta_{|\lambda_i|, n} \right\rangle \right\rangle_0 \quad (37)$$

where the expectation value

$$\langle \langle \mathcal{O}(\Lambda) \rangle \rangle_0 = \frac{\langle \langle \mathcal{O}(\Lambda) \delta_{u,v} \rangle \rangle}{\langle \langle \delta_{u,v} \rangle \rangle} \quad (38)$$

refers to the closed ‘vacuum’ graphs only. Further we have introduced and implemented the decomposition of each such graph Λ into individual closed loops

$$\Lambda = \bigcup_{i=1}^{|\Lambda|} \lambda_i \quad (39)$$

of lengths (number of link-lines) $|\lambda_i|$. In [17], inspired by percolation and random walk theory, the asymptotic scaling form

$$\ell_n \propto n^{-\tau} e^{-\theta n} \quad (40)$$

has been proposed introducing the loop tension θ and a power correction exponent τ . We found that such a fit describes reasonably well data that we have generated with S_q at $N = 4$ for correlations lengths $m^{-1} = 2 \dots 18$ and size $mL \approx 10$. Our aim here was not a high precision estimation of θ and τ . A clean assessment of their systematic errors would require quite some effort as it depends on the chosen fit window and their mutual correlation. We content ourselves at present with quoting that our analysis suggests that our data are roughly described by

$$\tau \approx 1.8, \quad \theta \approx m^2/17. \quad (41)$$

If we now pick a random 2-vertex we hit long loops more frequently and it will be part of a loop of length n with a probability proportional to $n\ell_n$. The cost to re-flag such a loop will hence on average be

$$\frac{\sum_n n^2 \ell_n}{\sum_k k \ell_k} \approx (2 - \tau)\theta^{-1}. \quad (42)$$

Because θ^{-1} grows roughly proportional to the *squared correlation length* in the continuum limit (‘fractal dimension two’) simulations with the R algorithm slow down asymptotically in a way similar to ordinary local methods. It is to be noted that this section of the code (the re-flag while-loop) is very simple and thus dominates on larger lattices only, and that loop simulations still have great advantages. In any case we have found that the CPU time per site for R grew roughly by a factor 60 as the correlation length and L are scaled up by a factor 7. Slower memory access on larger lattices may however also have entered here to some degree.

3.2.2 Elimination of slowing down

To proceed it was instructive to draw some analogies to Fortuin-Kastelyn cluster based algorithms for the q -state Potts model. In an early proposal Sweeny [18] has worked with bond variables only. The Boltzmann weight then contains a factor q^{N_c} , where N_c is the number of percolation clusters implied by the bond configuration. It resembles our weight $N^{|\Lambda|}$, for instance by allowing to analytically continue in q . During a local bond update nonlocal information is required: does the status of the single bond change N_c or not? This leads to the same kind of slowing down. Sweeny has designed a system of hierarchical express pointers to accelerate the travel around loops (like express trains of the New York subway). One could consider such an improvement also for R here.

A much simpler solution of the problem was however the one of Swendsen and Wang [1]. They keep spin *and* bond variables and update them in alternating order. One may actually view the cluster-wise assigned spins as just a device to stochastically dissolve the nonlocal weight into local steps. Transferring this technique to our problem at hand we insert, for example in (16), the representation

$$N^{|\Lambda|} = \sum_{\alpha_1=1}^N \dots \sum_{\alpha_{|\Lambda|=1}}^N 1 = \frac{N}{N-1} \sum_{\alpha}^{\prime} 1. \quad (43)$$

Here the enlarged phase space now consists of graphs Λ where each loop λ_i contained in it carries a label α_i that is freely summed over N values. The update is extended now to such configurations including a choice for all α_i . In the last (primed) sum we omit α assignments where the indices of the two active loops

coincide. The reason for this small extra twist will become clear soon. The loop partition function now reads for example

$$\mathcal{Z} = \int DU \mathcal{Y}[U] = \frac{N}{N-1} \sum_{\Lambda \in \mathcal{L}_2} \sum_{\alpha}' \rho^{-1}(u-v) W[\Lambda] \quad (44)$$

and expectation values in this ensemble are formed in the obvious way.

The simulation of the ensemble including the α values requires only minimal changes. The flag entries of the linked list are rededicated to now store the flavor values $\alpha \in \{1, 2, \dots, N\}$ of each vertex that is inherited from the loop to which it belongs. The extend/retract step I is completely unchanged, flavor is just passed on in extensions. The re-route step II (at fixed α) becomes even simpler now and proceeds as follows:

- II' If $u \neq v$ and $d(u) > 2$ holds we pick one of the 2-vertices at u . If it carries the same flavor as the initial 1-vertex of the uv loop we (always) swap in the way described before, otherwise nothing is done. Then the same is repeated for vu loop at u .

Because of the restriction $\alpha_{uv} \neq \alpha_{vu}$ it never happens that a re-route now leads to a line connecting for example $\overline{\phi^\dagger}(u)$ with $\phi(u)$, a contribution not included in our definition of the class \mathcal{L}_2 or $\overline{\mathcal{L}}_2$ designed such that u, v map out the *adjoint* correlation. The larger class would lead to a correlation with a singlet part decaying to a known constant instead of zero. It could be canceled but we would presumably be left with more and unnecessary noise.

For ergodicity we also have to periodically update the flavor assignments after a certain number of the steps just discussed. We expect the cost for one iteration to remain $O(V)$ if we do this only after $O(V)$ extend/retract steps. One obvious option for these new steps would be to identify all loops λ_i in Λ (including uv and vu) and re-flavor them randomly. Some thought shows however that for ergodicity it is already sufficient to only randomly re-flavor the two active loops to one of the $N(N-1)$ pairs $\alpha_{uv} \neq \alpha_{vu}$. We call this type of re-flavor step now III. Some short experiments identified the following combination as quite efficient

$$1 \text{ Iteration} = [(\text{I}_u \text{II}_u \text{I}_v \text{II}_v)^{V/2} \text{III}]^N. \quad (45)$$

In particular our experiments have shown that it is *not* profitable to re-flavor all loops. Most important, it was quite pleasant to find that the errors of relevant observables grow only by 10% or so if they are accumulated during the same number of such I-Iterations replacing the much more costly R-Iterations. A more detailed discussion of autocorrelations and (the absence of) critical slowing down will follow in the next section.

4 Numerical tests

We here report data on a number of simulations in $D = 2$ dimensions. The reason for this restriction is that physical interest in the $CP(N - 1)$ models and hence available data seem to be concentrated on this dimensionality. We expect our new formulation and algorithms to be generalizable to other dimensions without problems.

We have implemented the algorithms R and I as C codes. The graphs Λ are encoded into a linked list as described in detail in [10]. In C a very natural implementation uses structures of pointers that are dynamically created and erased. We have found however that the more static storage handling described in [10] offers slight advantages in speed and have hence returned to it in the final version.

4.1 Validation with the action S_q in large volumes

We first simulate the action S_q for $N = 4$ to become able to compare (and find consistency) with data in [16] [5] [6] on a lattice by lattice basis. These simulations are summarized in table 1. After each extend/retract we have continuously

β_q	L	χ	ξ_1	ξ_2	L/ξ_2	K
2.3	20	11.064(9)	2.5736(12)	2.6045(10)	7.7	2.59585(24)
2.5	32	26.214(28)	4.4491(27)	4.5097(23)	7.1	3.07843(18)
2.7	64	79.57(11)	8.7813(76)	8.9018(61)	7.2	3.57230(10)
2.9	128	275.13(50)	18.521(22)	18.837(18)	6.8	4.03968(6)
3.1	256	930.2(2.2)	38.087(62)	38.639(50)	6.6	4.48085(3)
3.3	512	2998.6(8.2)	74.80(16)	75.54(13)	6.8	4.90816(2)

Table 1: Results of simulations with the quartic action (17) that are immediately comparable to published data.

recorded the contributions to (23) and to the time slice correlations

$$G(t) = \langle\langle \rho(u - v)[\delta_{t,u_0-v_0} + \delta_{t,u_1-v_1}] \rangle\rangle \quad (46)$$

where the δ functions are L -periodic and we enhance the statistics by summing over both directions for $L_0 = L_1 \equiv L$. As discussed in [10] (see also [11]) we took $\rho(x)$ proportional to the free lattice propagator with a mass \hat{M} close to the one expected for the simulated lattice. From successive pairs of time slices we determine an effective mass by solving

$$\frac{G(t+1)}{G(t)} = \frac{\cosh(m(t+1 - L/2))}{\cosh(m(t - L/2))}, \quad \rightarrow m = m_{\text{eff}}(t + 1/2). \quad (47)$$

Following [16] correlation lengths $\xi_k = 1/m_{\text{eff}}(t_k + 1/2)$ are determined self-consistently such that $k\xi_k \in [t_k, t_k + 1]$, i.e. roughly at separations ξ and 2ξ .

In the column

$$K = \frac{1}{DV} \left\langle \left\langle \sum_{x\mu} k(x, \mu) \right\rangle \right\rangle_0 \quad (48)$$

we list the average number of lines per link in the simulated graphs. Actually there are K lines of either orientation. As in the $O(N)$ model (see [10]) K is a direct measure of the internal energy due to the identity

$$K = 2\beta_q \langle |\phi^\dagger(x)\phi(x + \hat{\mu})|^2 \rangle. \quad (49)$$

Each row in table 1 derives from 10^7 iterations of the I algorithm. We have stored our data as 10^5 blocks from 100 successive iterations each. With these blocks an ordinary error analysis with the tool [19] was carried out. Between these measurements, on average separated by 100 iterations, hardly any autocorrelations are detectable. The errors of our errors are thus at a percent level and all digits given in the tables are significant. In addition, using multicore PCs, we always simulate between 8 and 32 independent replica and monitor for acceptable Q-values [19].

To extract the number of loops $|\Lambda|$ in I-simulations one has to implement an additional observable to obtain this information. In our original R-simulations it is however available ‘for free’ and was measured. We have found values $|\Lambda|/V = 1.25 \dots 1.05$ slowly falling as β rises, thus $O(1)$ loop per site. The ‘historic’ parameter sets in table 1 have led to physical sizes of about $mL \approx 7$. We have found that this is too small to see a convincing mass-plateau at our present precision level. We have therefore repeated all runs on larger lattices $mL \approx 10$, see table 2. In figure 2 the effective mass on the largest lattice now shows a satisfactory plateau. Beyond the steep initial decay, we show only every sixth effective mass value to not clutter up the plot. The size of the relative statistical errors of m_{eff} is separation independent as expected [11]. The growth very close to $t = L/2$ has kinematic reasons since at $L/2$ the correlation has a minimum for any mass. We then decided on these larger lattices to quote mass values from a fit to the correlation over a window $t = L/4$ to $t = L/2$. This is the horizontal line error-band in figure 2. We refer to [10] for a discussion of the fitting procedure which we took over unchanged. The lattices of table 2 represent a scaling set where the lattice spacing changes toward the continuum ‘at fixed physics’. The weight ρ was formed with $\bar{M} = 10/L$. The optimal ρ is observable dependent. We repeated the run $L = 380$ with $\rho \equiv 1$. The resulting error in $\chi = 922.89(57)$ is about four times smaller while the error in $\xi = 38.089(33)$ went up by more than a factor two. The execution time *per site* of an I iteration between the first and the last line of table 2 still goes up by a (modest) factor 1.7, which is probably an effect of memory or

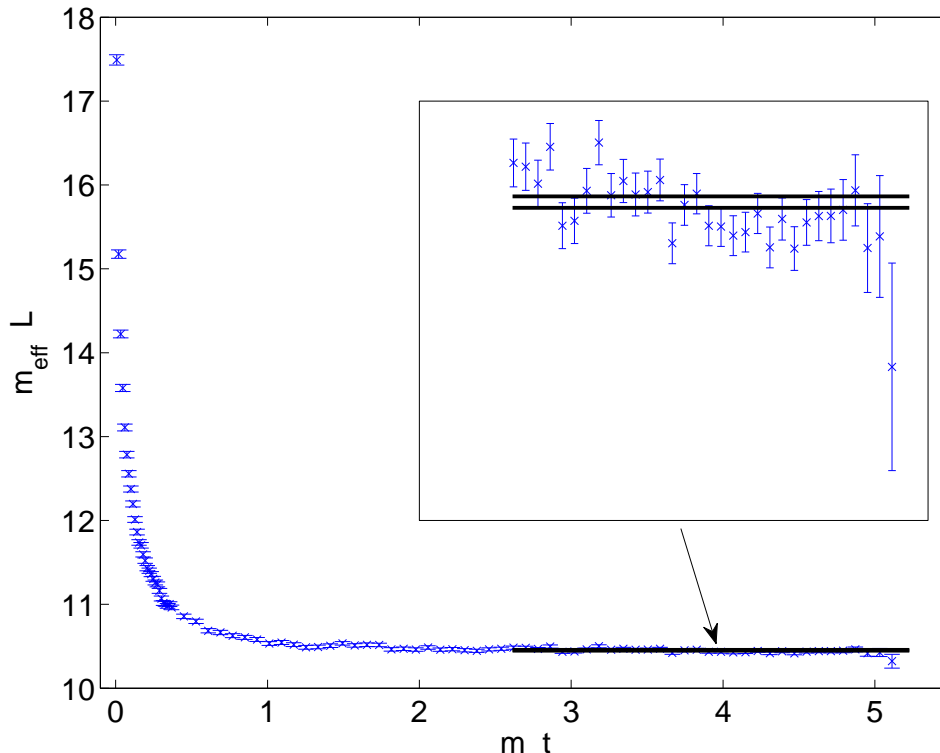


Figure 2: Effective mass as a function of time slice separation at $\beta_q = 3.3$ and $L = 780$.

cache access with 8 replica (cores) sharing the memory. The total CPU time of the run $L = 780$ was about 330 hours on one double-quadcore Xeon (2.27GHz).

We close on a warning side-remark. With all our observables being positive we originally thought that a single precision simulation (about 20 % faster) would be sufficient. We then found however that in plots like figure 2 the errorbars scattered around a smooth curve to a degree that seemed implausible. With the transition to double precision throughout (it was always used for the data analysis) this effect immediately went away. The mean value of the mass in single precision was still compatible with the new value while χ was found to be different beyond errors.

4.2 Autocorrelations

In ordinary simulations the errors of observables are influenced by both the variance of the quantity and by its integrated autocorrelation time. The latter depends

β	L	χ	$\xi(L/4 \rightarrow L/2)$	K
2.3	26	11.015(9)	2.5889(7)	2.59502(19)
2.5	44	26.015(29)	4.4561(13)	3.07771(14)
2.7	88	78.99(12)	8.8256(28)	3.57190(8)
2.9	188	272.78(53)	18.574(7)	4.03950(4)
3.1	380	926.4(2.4)	38.068(15)	4.48080(2)
3.3	780	2960.2(8.6)	74.619(32)	4.90818(1)

Table 2: Data from simulations of the CP(3) model with $mL = 10$. The mass $m = 1/\xi$ is determined by a fit to the correlation.

on the algorithm in use while the former is a property only of the ensemble to be simulated. This distinction tends to get blurred somewhat for our strong coupling simulations as already discussed in [11]. The point is that histograms like $\mathcal{O}(x) = \langle\langle \delta_{x,u-v} \rangle\rangle$ in the simplest case are measured continuously during the update. An extreme view for the R algorithm would be that after each microstep, for example $I_u II_u$ in (34), we in this way measure all $\mathcal{O}(x)$ (mostly implicit zero contributions). Then the usual division holds and we could obtain τ_{int} in units of microsteps, but would need to handle lots of data for this purpose. In practice we block however $O(V)$ such measurements and then both the variance of the blocks and the residual autocorrelations between them depend on the underlying algorithm's ‘decorrelation power’.

With this explained we cite some autocorrelation times for the I algorithm. To that end we have repeated the simulations of table 2 with only 10^6 iterations but storing the contribution for each of them separately (in particular all $G(t)$). Then an ordinary analysis [19] yields autocorrelation times in units of iterations (computational complexity $O(VN)$, like ‘sweeps’). Results are given in figure 3. The dotted lines just connect data points for the same observable. Here $\tau_{\text{int},m}$ refers to the fitted masses. Values based on $m_{\text{eff}}(L/4)$ cannot be shown as they would fall on top of $\tau_{\text{int},\chi}$, i.e. be close to $1/2$ for all lattices which means no autocorrelations in our definition of τ_{int} . We here see the complete absence of any growth of τ_{int} as the continuum limit is taken. The slowest modes couple to the total graph-size K which however even speeds up in the continuum limit. In any case, the most naive (and important) conclusion from table 2 is simply, that we see an approximately constant relative error in ξ with costs only growing linearly with the number of sites.

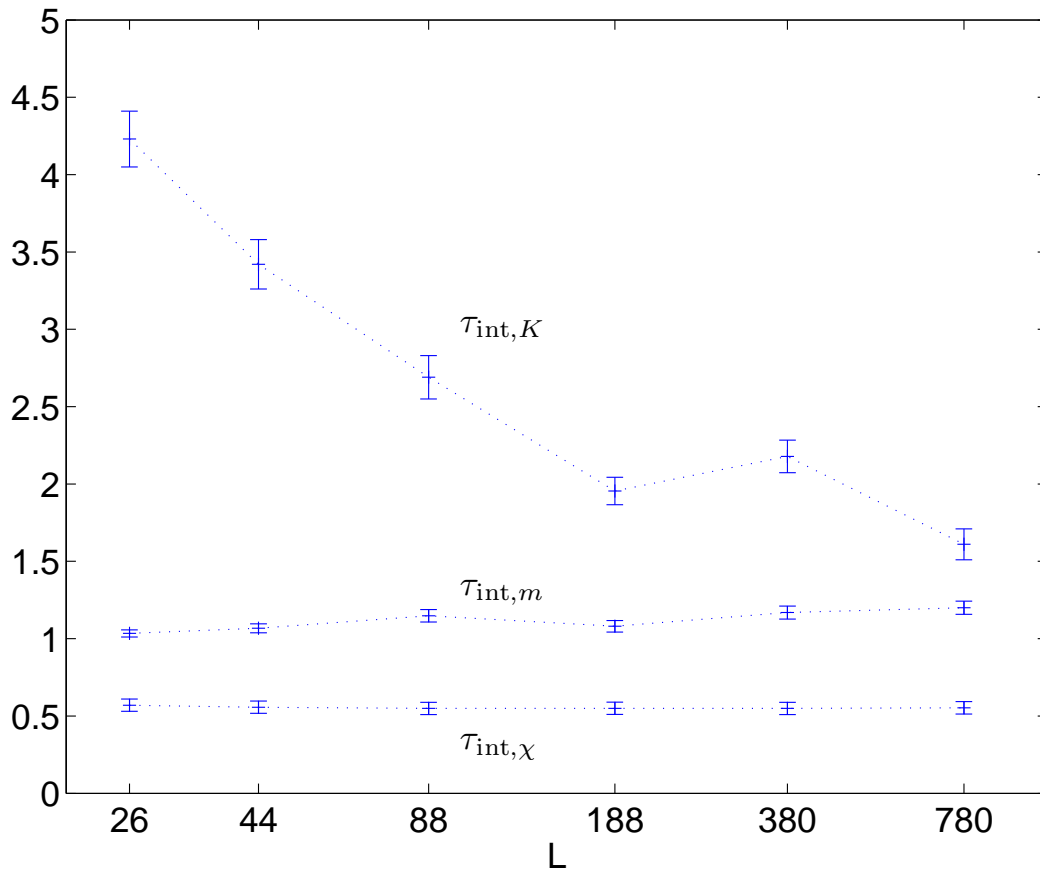


Figure 3: Integrated autocorrelation times in units of I-iterations.

4.3 Universality and finite size scaling

We conducted another series of tests for the $N = 3$ model in a finite size scaling situation. To compare with data in [7] we here switch to the second moment definition of the mass m_2 . It is based on ratios of momentum space correlations which can be measured in the loop ensemble by

$$\tilde{G}(p) \propto \langle\langle \rho(u-v) \cos(p \cdot (u-v)) \rangle\rangle \quad (50)$$

which follows from Fourier transforming (21). Table 3 contains our new data.

We consider the step scaling function [20] $z(2L)$ versus $z(L)$ for

$$z(L) = m_2(L) \times L \quad (51)$$

with pairs $(L, 2L)$ at the same β . For large enough L this graph is expected to reach a universal continuum curve. Rather than tuning the smaller lattices as

act.	β_\times	$m_2(L)L _{L=32}$	$m_2(L)L _{L=64}$	$m_2(L)L _{L=128}$
S_q	2.25	2.3979(18)	3.6582(22)	7.2640(30)
S_q	2.4	1.9896(18)	2.4133(19)	3.6631(24)
S_q	2.5	1.8351(18)	2.1080(19)	2.6905(21)
S_q	3.0	1.4285(19)	1.5286(20)	1.6575(20)
S	4.0	2.1138(17)	2.6974(19)	4.6179(26)
S	4.2	1.9366(17)	2.2812(19)	3.1972(22)
S	4.5	1.7499(18)	1.9646(19)	2.3433(20)
S	5.0	1.5448(18)	1.6747(19)	1.8607(20)

Table 3: Finite volume results for $L = 32, 64, 128$ with actions (17) and (1).

in [10] we here give only a more qualitative ‘curve-collapsing’ demonstration. In figure 4 we show the pairs contained in table 3 together with data¹ from refs. [7], [8] using their lattice pairs between (32, 64) and (104, 208) produced with standard simulations using S_q at $\beta_q = 2.25, 2.5$. We see a very convincing close to universal curve. Some remaining ‘roughness’ from lattice artefacts expected at a level L^{-2} can just still be anticipated, for example around $z(L) \approx 2.4$.

5 Topological charge in the loop model

In two dimensions the gauge field $U(x, \mu)$ gives rise to an integer topological charge Q . It has a straight-forward definition on the lattice and we may hence extend the action by the θ term by including the phase $\exp(i\theta Q)$ with the U integrations.

We parameterize

$$U(x, \mu) = e^{iA_\mu(x)}, \quad A_\mu(x) \in (-\pi, \pi] \quad (52)$$

and define the field strength

$$F_{\mu\nu} = \partial_\mu A_\nu - \partial_\nu A_\mu \in (-4\pi, 4\pi]. \quad (53)$$

An integer topological charge density $n_{\mu\nu}$ is then extracted by setting

$$F_{\mu\nu} = [F_{\mu\nu}] + 2\pi n_{\mu\nu}, \quad [F_{\mu\nu}] \in (-\pi, \pi] \quad (54)$$

and the global charge is given by

$$Q = \sum_x n_{01}(x). \quad (55)$$

¹I would like to thank the authors of [8] for sending their data and allowing me to reproduce them here.

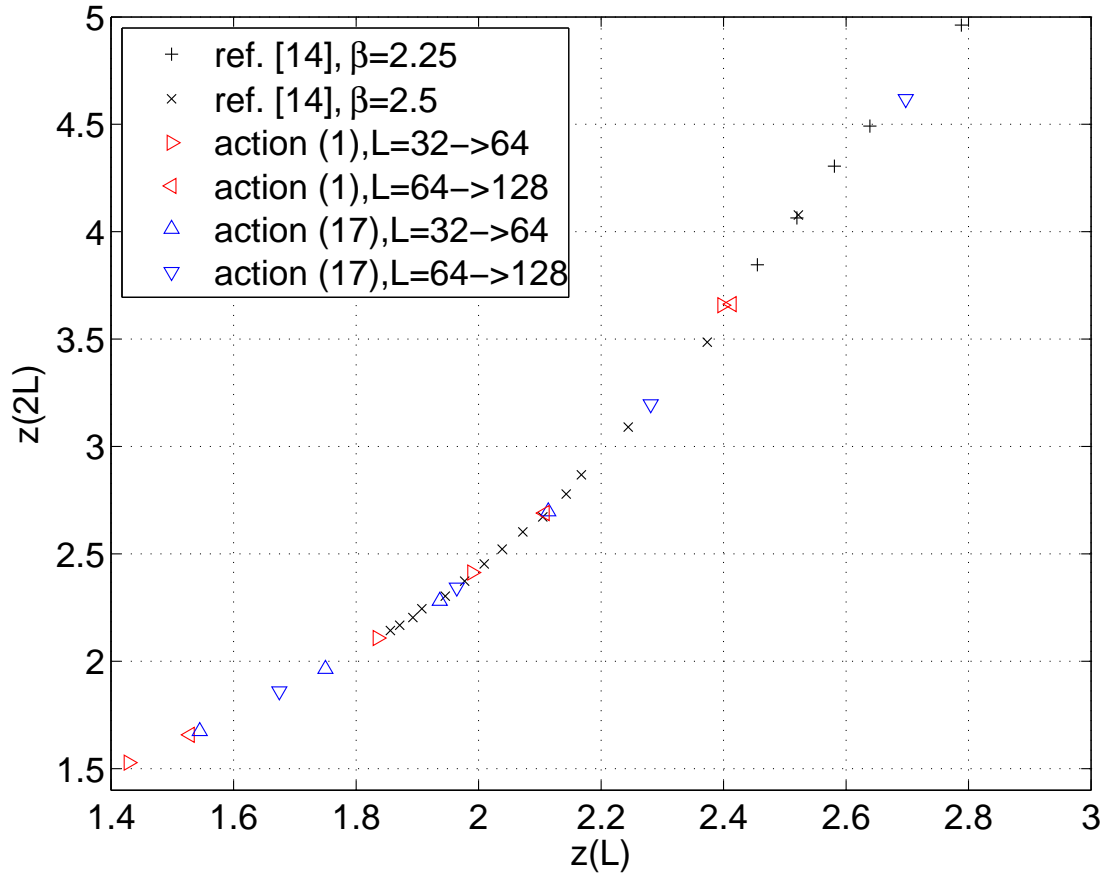


Figure 4: Finite size scaling function of the CP(2) model with data from two different actions and spin as well as loop simulations. Errors (horizontal and vertical) are at most comparable to the symbol sizes.

We next Fourier expand

$$e^{i\bar{\theta}[F_{01}]} = \sum_{h=-\infty}^{\infty} H(\bar{\theta}; h) e^{ih[F_{01}]} = \sum_{h=-\infty}^{\infty} H(\bar{\theta}, h) e^{ihF_{01}} \quad (56)$$

with $\bar{\theta} = \theta/(2\pi)$ and

$$H(\bar{\theta}; h) = \frac{\sin[(\bar{\theta} - h)\pi]}{(\bar{\theta} - h)\pi} = \frac{\sin(\theta/2)}{\theta/2} (-1)^h \frac{\theta}{\theta - 2\pi h}. \quad (57)$$

We remark that H is precisely the kernel that appears in connection with the sampling theorem [21]. There a continuous time signal with compact support in

frequency space is reconstructed from its values at equidistant discrete times. In our case $\bar{\theta}$ is continuous and the critical Nyquist sampling frequency is one in our units. If $\bar{\theta}$ gets close to an integer k we have

$$H(k + \epsilon; h) = \delta_{kh} \quad (58)$$

in a distribution sense [first insert H into a sufficiently convergent sum, then take $\epsilon \rightarrow 0$]. If we now promote h to a field $h(x)$, use $\sum_x F_{\mu\nu} = 0$ and rearrange the $U(x, \mu)$ from plaquettes into in a link-wise order we arrive at

$$e^{i\theta \sum_x n_{01}(x)} = \sum_h \left[\prod_x H(\bar{\theta}; h(x)) \right] \prod_{x\mu} [U(x, \mu)]^{-\varepsilon_{\mu\nu} \partial_\nu^* h(x)} \quad (59)$$

where $\varepsilon_{\mu\nu}$ is the antisymmetric tensor with $\varepsilon_{01} = +1$.

The expression

$$\Theta = \int DU e^{i\theta Q} \prod_{x\mu} U^{j(x, \mu)} = \sum_h \left[\prod_x H(\bar{\theta}; h(x)) \right] \prod_{x\mu} \delta_{j_\mu(x), \varepsilon_{\mu\nu} \partial_\nu^* h(x)} \quad (60)$$

is now well-prepared for its use in (14) and leads to

$$\mathcal{Z}_\theta = \sum_{\Lambda \in \bar{\mathcal{L}}_2} \rho^{-1}(u - v) W[\Lambda] N^{|\Lambda|} \Theta[\Lambda], \quad (61)$$

where Θ depends on the integer flux $j(x, \mu)$ which we here regard as a function of Λ . The set $\bar{\mathcal{L}}_2$ is such that flux conservation (12) holds, which is a necessary condition for the constraint in Θ to have solutions.

In [22] a very nice discussion is given for a closely related representation of σ -models which we adopt now. The field $h(x)$ is really associated with plaquettes, or sites in the dual lattice. Its integer values in an h configuration may be viewed as the height of a tower above (or below) its plaquette, like a ‘lego-plot’ of the experimentalists. Then the euclidean plane is decomposed into domains of equal height. Due to the constraint in (60) the links along their boundaries carry nonvanishing conserved flux $j(x, \mu)$ whose value and sign is determined by the difference between the domains heights on both sides. As noted in [22] this is a solid-on-solid model with additional interactions. In the limit $\theta \rightarrow 0$ only $h(x) = 0$ survives. At $\theta = \pi$ on the other hand there is a reflection symmetry $h(x) - 1/2 \leftrightarrow -(h(x) - 1/2)$.

We leave it to a future investigation to decide if or at which (β, θ) in spite of the sign oscillations in the weight H it is possible to numerically investigate topology in the loop version of the $CP(N - 1)$ model.

6 Conclusions

We have constructed a loop re-formulation of the $CP(N - 1)$ model which required just a rather straight-forward extension of the steps used in the $O(N)$ model in [10]. With only minor changes we could obtain the transcription for both the quartic lattice action and for the formulation involving an additional $U(1)$ gauge field. For the numerical simulation an important refinement was necessary to avoid critical slowing down in the $CP(N - 1)$ case: the stochastic rather than exact treatment of the weight $N^{|\Lambda|}$ where $|\Lambda|$ is the number of closed loops in an arbitrary strong coupling graph. The exact algorithm could still be used to simulate the theory also at non-integer N , if desired, although with accepting some critical slowing down.

One of the main reasons to invent and study the $CP(N - 1)$ models was their analogy with Yang-Mills theory in four dimensions with regard to both asymptotic freedom and the existence of an integer winding number. As we have argued that the loop model is an exact representation of the original model the observables related to topology should possess an image in the loop model. We have constructed the effect of the term in the action related to the θ parameter. It leads however to the appearance of negative weights in the loop model. It is deferred to future work to find out in which parameter range, by including the signs in observables or by further re-formulation, numerical calculations are possible.

Acknowledgments: I would like to thank Tomasz Korzec and Peter Weisz for discussions and Burkhard Bunk and Stefan Schaefer for advice with computing and C. Financial support of the DFG via SFB transregio 9 is acknowledged.

References

- [1] R. H. Swendsen, J.-S. Wang, Nonuniversal critical dynamics in Monte Carlo simulations, *Phys. Rev. Lett.* 58 (1987) 86.
- [2] U. Wolff, Collective Monte Carlo Updating for Spin Systems, *Phys. Rev. Lett.* 62 (1989) 361.
- [3] K. Jansen, U.-J. Wiese, Cluster algorithms and scaling in $CP(3)$ and $CP(4)$ models, *Nucl. Phys.* B370 (1992) 762.
- [4] S. Caracciolo, R. G. Edwards, A. Pelissetto, A. D. Sokal, Wolff type embedding algorithms for general nonlinear sigma models, *Nucl. Phys.* B403 (1993) 475.
- [5] M. Hasenbusch, S. Meyer, Testing accelerated algorithms in the lattice CP^{*3} model, *Phys. Rev.* D45 (1992) 4376.

- [6] M. Hasenbusch, S. Meyer, Does the topological charge scale in the lattice CP(3) model?, Phys. Lett. B299 (1993) 293.
- [7] B. B. Beard, M. Pepe, S. Riederer, U. J. Wiese, Study of CP(N-1) Theta-vacua by cluster-simulation of SU(N) quantum spin ladders, Phys. Rev. Lett. 94 (2005) 010603.
- [8] B. B. Beard, M. Pepe, S. Riederer, U. J. Wiese, Efficient cluster algorithm for CP(N-1) models, Comput. Phys. Commun. 175 (2006) 629.
- [9] N. Prokof'ev, B. Svistunov, Worm Algorithms for Classical Statistical Models, Phys. Rev. Lett. 87 (16) (2001) 160601.
- [10] U. Wolff, Simulating the All-Order Strong Coupling Expansion III: O(N) sigma/loop models, Nucl. Phys. B824 (2010) 254, Erratum in preparation, arXiv: 0908.0284v3
- [11] U. Wolff, Simulating the All-Order Strong Coupling Expansion I: Ising Model Demo, Nucl. Phys. B810 (2009) 491.
- [12] U. Wolff, Precision check on triviality of ϕ^4 theory by a new simulation method, Phys. Rev. D79 (2009) 105002.
- [13] P. Di Vecchia, A. Holtkamp, R. Musto, F. Nicodemi, R. Pettorino, Lattice CP**(N-1) Models and their large N behavior, Nucl. Phys. B190 (1981) 719.
- [14] E. Domany, D. Mukamel, B. Nienhuis, A. Schwimmer, Duality relations and equivalences for models with O(N) and cubic symmetry, Nucl. Phys. B190 (1981) 279.
- [15] B. Nienhuis, Exact critical point and critical exponents of O(n) models in two-dimensions, Phys. Rev. Lett. 49 (1982) 1062.
- [16] U. Wolff, Scaling topological charge in the CP**3 spin model, Phys. Lett. B284 (1992) 94.
- [17] W. Janke, T. Neuhaus, A. M. J. Schakel, Critical Loop Gases and the Worm Algorithm, Nucl. Phys. B829 (2010) 573.
- [18] M. Sweeny, Monte Carlo study of weighted percolation clusters relevant to the Potts models, Phys. Rev. B 27 (1983) 4445.
- [19] U. Wolff, Monte Carlo Errors with less Errors, Comput. Phys. Commun. 156 (2004) 143.

- [20] M. Lüscher, P. Weisz, U. Wolff, A Numerical Method to compute the running Coupling in asymptotically free Theories, Nucl. Phys. B359 (1991) 221.
- [21] W. H. Press, B. P. Flannery, S. A. Teukolsky, W. T. Vetterling, Numerical Recipes: The Art of Scientific Computing, Cambridge Univ. Press, Cambridge.
- [22] I. Affleck, Nonlinear sigma model at $\Theta = \pi$: Euclidean lattice formulation and solid-on-solid models, Phys. Rev. Lett. 66 (1991) 2429.